



THE UNIVERSITY *of* EDINBURGH

## Edinburgh Research Explorer

# Ribonucleotide excision repair is essential to prevent squamous cell carcinoma of the skin

### Citation for published version:

Hiller, B, Hoppe, A, Haase, C, Hiller, C, Schubert, N, Müller, W, Reijns, MAM, Jackson, AP, Kunkel, TA, Wenzel, J, Behrendt, R & Roers, A 2018, 'Ribonucleotide excision repair is essential to prevent squamous cell carcinoma of the skin', *Cancer Research*. <https://doi.org/10.1158/0008-5472.CAN-18-1099>

### Digital Object Identifier (DOI):

[10.1158/0008-5472.CAN-18-1099](https://doi.org/10.1158/0008-5472.CAN-18-1099)

### Link:

[Link to publication record in Edinburgh Research Explorer](#)

### Document Version:

Peer reviewed version

### Published In:

Cancer Research

### General rights

Copyright for the publications made accessible via the Edinburgh Research Explorer is retained by the author(s) and / or other copyright owners and it is a condition of accessing these publications that users recognise and abide by the legal requirements associated with these rights.

### Take down policy

The University of Edinburgh has made every reasonable effort to ensure that Edinburgh Research Explorer content complies with UK legislation. If you believe that the public display of this file breaches copyright please contact [openaccess@ed.ac.uk](mailto:openaccess@ed.ac.uk) providing details, and we will remove access to the work immediately and investigate your claim.



# **Ribonucleotide excision repair is essential to prevent squamous cell carcinoma of the skin.**

(Running title: Loss of RNase H2 causes skin cancer.)

Björn Hiller<sup>1#</sup>, Anja Hoppe<sup>2#</sup>, Christa Haase<sup>2</sup>, Christina Hiller<sup>2</sup>, Nadja Schubert<sup>3</sup>, Werner Müller<sup>4</sup>, Martin A. M. Reijns<sup>5</sup>, Andrew P. Jackson<sup>5</sup>, Thomas A. Kunkel<sup>6</sup>, Jörg Wenzel<sup>7</sup>, Rayk Behrendt<sup>2##</sup>, Axel Roers<sup>2##</sup>

<sup>1</sup>Gene Center and Department of Biochemistry, Ludwig-Maximilians-Universität München, 81377 Munich, Germany

<sup>2</sup>Institute for Immunology, Medical Faculty Carl Gustav Carus, TU Dresden, 01307 Dresden, Germany

<sup>3</sup>Institute for Biochemistry, Charité Universitätsmedizin Berlin, 10117 Berlin, Germany

<sup>4</sup>Faculty of Biology, Medicine and Health, University of Manchester, Manchester M13 9PT, United Kingdom

<sup>5</sup>MRC Human Genetics Unit, MRC Institute of Genetics and Molecular Medicine, The University of Edinburgh, Edinburgh, UK.

<sup>6</sup>Genome Integrity and Structural Biology Laboratory, National Institute of Environmental Health Sciences (NIEHS), National Institutes of Health (NIH), Research Triangle Park, NC, USA.

<sup>7</sup>Department of Dermatology and Allergy, University Hospital Bonn, Bonn, Germany.

#equal contribution

## Abbreviations:

AGS	Aicardi-Goutières syndrome
BMMRD	biallelic mismatch repair deficiency
DDR	DNA damage response
ISGs	interferon-stimulated genes
KIN	keratinocyte intraepithelial neoplasia
MMR	mismatch repair
RER	ribonucleotide excision repair
RNase H2	ribonuclease H2
SSC	squamous cell carcinoma

## Corresponding authors:

Axel Roers and Rayk Behrendt

Institute for Immunology

Medical Faculty Carl Gustav Carus

TU Dresden

Fetscherstr. 74

01307 Dresden

[axel.roers@tu-dresden.de](mailto:axel.roers@tu-dresden.de), [rayk.behrendt@tu-dresden.de](mailto:rayk.behrendt@tu-dresden.de)

phone: 0049 351 458 6500

fax: 0049 351 458 6316

The authors declare no potential conflicts of interest.

## **Abstract**

Due to imperfect discrimination against ribonucleoside triphosphates by the replicative DNA polymerases, large numbers of ribonucleotides are incorporated into the eukaryotic nuclear genome during S-phase. Ribonucleotides, by far the most common DNA lesion in replicating cells, destabilize the DNA, and an evolutionarily conserved DNA repair machinery, ribonucleotide excision repair (RER), ensures ribonucleotide removal. Whereas complete lack of RER is embryonically lethal, partial loss-of-function mutations in the genes encoding subunits of RNase H2, the enzyme essential for initiation of RER, cause the SLE-related type I interferonopathy Aicardi-Goutières syndrome. Here we demonstrate that selective inactivation of RER in mouse epidermis results in spontaneous DNA damage and epidermal hyperproliferation associated with loss of hair follicle stem cells and hair follicle function. The animals developed keratinocyte intraepithelial neoplasia and invasive squamous cell carcinoma with complete penetrance, despite potent type I interferon production and skin inflammation. These results suggest that compromises to RER-mediated genome maintenance might represent an important tumor-promoting principle in human cancer.

## **Statement of Significance**

Selective inactivation of ribonucleotide excision repair by loss of RNase H2 in the murine epidermis results in spontaneous DNA damage, type I interferon response, skin inflammation, and development of squamous cell carcinoma.

## Introduction

Genome integrity is continuously challenged by a multitude of different hazards that cause a broad spectrum of different lesions in DNA [1]. Spontaneous hydrolysis, ionizing radiation, exogenous chemicals and endogenous metabolites, including reactive oxygen species, inflict cumulative damage to DNA [1]. Fortunately, various DNA repair pathways revert most of this damage, thereby dramatically slowing down age-related deterioration of DNA integrity and suppressing the development of cancer [2]. In addition to continuous, time-dependent harm to DNA, other forms of damage are introduced already during replication by errors the replicative polymerases make, despite their remarkable fidelity. Such replication errors include incorporation of deoxyribonucleotides that are not complementary to the template, which occurs every  $10^4$ - $10^6$  bases, depending on the DNA polymerase. Most mismatched nucleotides are removed by the proofreading activity that some DNA polymerases possess, while the remaining mismatches are detected and corrected by DNA mismatch repair (MMR), which is directly coupled to the replication machinery [3-5]. Postreplicative mismatch repair is an important tumor-suppressive principle as genetic defects in MMR proteins cause cancer predisposition syndromes, including Lynch syndrome [6] and biallelic mismatch repair deficiency (BMMRD) syndrome [7].

Another form of replication error is the incorporation of nucleotides containing the correct base, but the wrong sugar. For example, discrimination between incoming deoxyribonucleotides (dNTPs) and ribonucleotides (rNTPs) is imperfect for the three DNA polymerases that replicate the vast majority of the undamaged eukaryotic nuclear genome [8], resulting in frequent incorporation of rNMPs into genomic DNA [9, 10]. The probability for this mistake is increased by the far greater cellular abundance of rNTPs compared to dNTPs [8, 11] such that on average, more than  $10^6$  rNMPs are incorporated during one round of replication of a mammalian genome [12]. Newly incorporated rNMPs destabilize DNA [10] and pose a major threat to genome integrity due to their reactive 2'OH group. A highly conserved repair pathway, ribonucleotide excision repair (RER), ensures their removal [10, 13, 14]. Like MMR, RER may be directly coupled to replication and results in rapid postreplicative repair of rNMPs. The first step in RER is detection of rNMPs embedded in the DNA double helix by ribonuclease H2 (RNase H2). RNase H2 then incises the rNMP-containing strand immediately 5' of the rNMP. *In vitro*, this is followed by strand displacement synthesis by pol $\delta$  or pol $\epsilon$ , flap cleavage by Fen1 or Exo1 and ligation of the nick [14]. Interestingly, during their brief transient presence in DNA, rNMPs seem to serve important physiological functions in DNA metabolism [8, 13, 15]. They may provide a strand discrimination signal in MMR for the nascent leading strand [16, 17], wherein RNase H2-mediated incisions, occurring only in the newly synthesized rNMP-containing strand may serve as entry points for MMR enzymes. Moreover, nicking by RNase H2 could be crucial for

relaxing leading strand torsional stress [18]. rNMPs might also be incorporated during repair synthesis occurring in non-cycling cells that contain very high rNTP:dNTP ratios.

RNase H2-deficient cells are incapable of executing normal RER, carry high numbers of rNMPs in their DNA and spontaneously mount a DNA damage response (DDR), reflecting the DNA-destabilizing effects of rNMPs (reviewed in [13, 15, 19]). rNMPs alter DNA structure and thereby potentially affect multiple key DNA transactions. rNMPs increase the rate of spontaneous hydrolysis and were shown to trigger a mutagenic repair pathway in yeast depending on DNA topoisomerase 1, which, like RNase H2, can incise at single rNMPs, potentially generating unligatable ends in repetitive DNA that result in short deletion mutations [20]. Topoisomerase 1 cleavage at ribonucleotides embedded in the DNA can also result in double strand breaks and replication stress ensuing from abnormally long-lived topoisomerase 1-DNA complexes [21]. Moreover, bypassing rNMPs in DNA may pose a problem for replicative polymerases, that may result in replication fork stalling, strand breaks and replicative stress. In addition to genome protection by RNase H2-mediated removal of single rNMPs, RNase H2 contributes to genome stability also by resolution of R-loops [22], preventing damage resulting from collisions of RNA polymerases or replication forks with R-loops.

Loss of RNase H2 causes genome instability in yeast with high rates of gross chromosomal rearrangements and copy number variations (reviewed in [13]). Mammalian cells lacking the enzyme display increased numbers of strand breaks, activation of DNA damage responses (DDRs), and chromosomal aberrations [12, 23]. Abnormal mitotic chromosome segregation associated with this damage was shown to occur in RNase H2-deficient cells, leading to formation of micronuclei [24, 25]. Similarly, DNA damage can lead to herniation of chromatin into the cytosol [26]. Micronuclei and herniated chromatin expose large amounts of chromosomal DNA to the cytosolic DNA sensor cGAS that activates STING and thereby triggers an inflammatory response, including upregulation of interferon-stimulated genes (ISGs) and inflammatory cytokine production [24]. Unbalanced type I IFN responses are likely responsible for chronic inflammation in patients suffering from the rare monogenic autoimmune disorder Aicardi-Goutières syndrome (AGS), which can be caused by partial loss of function of RNase H2 or by mutations in other enzymes involved in nucleic acid metabolism [27, 28].

In mouse models, the effects of targeted inactivation of RNase H2 *in vivo* were found to critically depend on the degree to which RNase H2 activity was reduced. The RNase H2 complex is composed of three proteins, RNASEH2A, B and C all of which are essential for RNase H2 activity [29, 30]. Biallelic null or hypomorphic mutations in RNase H2 genes that cause massive reduction of activity resulted in embryonic or perinatal lethality associated with spontaneous DNA damage and activation of DDRs [12, 23, 31]. In contrast, a

homozygous mutation reducing RNase H2 activity to about 30% of wildtype levels triggered a spontaneous low level IFN response, but was not associated with gross pathology [32].

To elucidate consequences of severe RER deficiency for the homeostasis of a tissue with rapid cell turnover in adult animals, we bypassed embryonic lethality of ubiquitous RNase H2 deficiency by conditional gene inactivation. We demonstrate that complete loss of RNase H2 in skin epithelium results in spontaneous DNA damage and epidermal hyperproliferation that progresses to skin cancer with 100% penetrance, despite potent spontaneous type I IFN responses, demonstrating that RNase H2-dependent RER is an important tumor-suppressive principle.

## Material and Methods

**Mice.** *Rnaseh2b*<sup>FL/FL</sup> [23], *K14-Cre* [33], *Ifnar1*<sup>-/-</sup> (generated from *Ifnar1*<sup>FL</sup> mice [34] by ubiquitous deletion of the loxP-flanked fragment), *Trp53*<sup>-/-</sup> [34] were either on the C57BL/6NJ background or backcrossed for at least five generations to C57BL/6NJ. Mice were housed at the Experimental Center, Medical Faculty Carl Gustav Carus, TU Dresden, under specific pathogen-free conditions. All procedures were in accordance with institutional guidelines on animal welfare and were approved by the Landesdirektion Dresden (permit number 24-1/2013-12).

**Quantification of mRNAs by quantitative RT-PCR.** Total RNA was isolated using the NucleoSpin kit (Macherey-Nagel) according to the manufacturer's instructions. cDNA was generated using the RevertAid H Minus First Strand cDNA Synthesis kit (Thermo Fisher Scientific). Quantification of transcripts was performed on a Mx3005P QPCR system (Agilent Technologies) using the Maxima SYBR green/ROX qPCR Master Mix (Thermo Fisher Scientific). The following oligos were used: *Oas1* up, 5'-GCAATCCACAGCGATATCC-3'; *Oas1* down, 5'-CAACTGCTCACTGTCCACGG-3'; *Ifi44* up, 5'-GAGTCACTCATTCTCGGACTCCGC-3'; *Ifi44* down, 5'-GAGCGGGCATTGAAGTAAGGGC-3'; *Viperin* up, 5'-TTCGCCCGCATCAAAGCCGT-3'; *Viperin* down, 5'-AGGGGGCAGCGG-AAGTCGAT-3'; *Rnaseh2b* up, 5'-AGGTTTCCAGGGACAAGGAAGAGGA-3'; *Rnaseh2b* down, 5'-GTCAATGAAGCTGGAGTTCTGGAAG-3'; *Tbp1* up, 5'-TGACCCAGATCATGTTTGAGACCTTCA-3'; and *Tbp1* down, 5'-GGAGTCCATCACAATGCCTGTGG-3'. All samples were run in triplicates. qRT-PCR data are displayed as fold change compared to means of the respective control groups ± SD.

**Assay for RNase H2 activity.** Cell lysates were prepared and assayed for specific cleavage of an 18-bp double-stranded DNA substrate containing a single ribonucleotide in one strand as previously described [27, 29]. RNase H2-specific activity was determined by subtracting the cellular activity against a sequence-matched DNA duplex without ribonucleotides. Cell lysate protein concentration was determined and lysates were added to the reaction mix at a

final protein concentration of 100 ng/μl.

**Isolation and flow cytometric analysis of epidermal cells.** Back skin was excised and adipose tissue was removed. The skin was placed on a layer of trypsin solution (0.25%, Life Technologies Germany) with the epidermal side facing upwards. After incubation for 2 hours, the epidermis was separated from the dermis using blunt forceps. The epidermis was minced with scalpels and digested in 10 ml trypsin solution (0.25%, Life Technologies) for another hour. The digest was stopped by adding an equal volume of medium (DMEM (2/3) + HAM's F12 (1/3)) supplemented with 10% calcium free FBS and the cells were strained through a 40 μm nylon mesh. Cells were then centrifuged for 8 min at 500 g at RT and the pellet was resuspended in 2 ml FACS buffer. Epidermal stem cell populations were stained according to Jensen et al. [35]. For flow cytometry, cells were stained using the following antibodies: anti-CD45-FITC (1:400, eBioscience), anti-CD49f-PE (1:200, eBioscience), anti-CD34-eF660 (1:50, eBioscience), anti-Sca1-PerCP-Cy5.5 (1:200, eBioscience), anti-CD117-APC-Cy7 (1:800, Biolegend). Cell sorting and analysis was performed on an ARIA III cell sorter (BD) and data were recorded using DIVA software (BD) and analyzed using FlowJo (FlowJo, LLC).

**Transcriptome analysis.** Keratinocytes (CD49f<sup>+</sup>) and hematopoietic cells (CD45<sup>+</sup>) were isolated from skin cell suspensions by FACS (see above). Total RNA was isolated using the RNeasy Mini Kit+ (Qiagen). mRNA libraries were prepared and subjected to deep sequencing on an Illumina®HighSeq. Reads were mapped to the reference genome mm10 (Ensembl Version 75) using *gsnap* (v.2014-12-06 for analysis of CD45<sup>-</sup>CD49f<sup>+</sup> cells, v.2014-12-17 for analysis of CD45<sup>+</sup> cells) and genes were counted with *featurecount* v.1.4.6.. Differentially expressed genes (DEGs) were identified using DESeq2 v1.8.1 [36]. Clustering of DEGs into specific pathways was investigated using KEGG (<http://www.genome.jp/kegg/pathway.html>), Reactome (<https://reactome.org/>) and Interferome V2.0 ([www.interferome.org/](http://www.interferome.org/)) databases as well as the Ingenuity Pathway Analysis (IPA) software (Qiagen). RNA-seq data reported in this paper are accessible as a super series from the Gene Expression Omnibus database (GEO) under accession number GSE115005.

**Histology.** Formalin-fixed and paraffin-embedded skin sections were de-paraffinized and rehydrated, subjected to antigen retrieval (20 min 98°C in sodium citrate pH 6.0) and washed three times in TBST (1xTBS, 0.1% Triton X-100).

For quantification of phosphorylated histone H2A.X (γH2A.X), sections were blocked for 1h (10% goat serum in TBST) and incubated at 4°C over night with a phospho-histone H2A.X (pSer139) antibody (Cell Signaling, 1:50 in 1% goat serum/tris-buffered saline with 0.05% Tween20 (TBST)). Next, sections were washed (TBST) and incubated with a goat anti-rabbit-AF488 antibody (1:500, Thermo Fisher Scientific) for 4h at room temperature in the dark. After washing, nuclei were counterstained with DAPI in the mounting solution. Images were recorded on a Zeiss Axiovert ApoTome II and analyzed using Zen® software (Zeiss). γH2A.X

foci in at least 220 keratinocyte nuclei of the interfollicular epidermis per section were counted.

For quantification of Ki67-positive cells, endogenous peroxidase activity was blocked (3% H<sub>2</sub>O<sub>2</sub>, 20 min in the dark), unspecific epitopes were blocked (PBS 10% BSA, 0.5% Triton X-100 for 1h at room temperature) and sections were washed and incubated at 4°C over night with anti-Ki67-Biotin (eBioscience, 1:100 in PBS 1% BSA, 0.05% Triton X-100). After washing, sections were incubated for 1h at RT with HRP-conjugated Streptavidin (Dako, 1:300, PBS, 1% BSA, 0.05% Triton X-100). After addition of DAB mix (Vector Labs) and counter-staining with hematoxylin, Ki67-positive keratinocytes were counted in interfollicular epidermis.

For quantification of dying cells positive for activated caspase 3, antigen retrieval was performed in PBS with 1 mM EDTA, 0.05% Tween 20, pH 8.0 for 20 min in a pressure cooker), sections were blocked (PBS, 0.1% Tween 20, 5% normal goat serum) and incubated with rabbit anti-active-Caspase3 AF835 (R&D, 1:600) at 4°C over night, followed by washing and incubation for 1h at RT with goat anti-rabbit AF488 (ab150077, Abcam, 1:500). Nuclei were stained with DAPI. Images were recorded on a Keyence BZ-X710 microscope and positive cells were counted in interfollicular epidermis and follicular infundibula.

Histological evaluation was performed by a professional dermato-histopathologist (J. Wenzel, Bonn, Germany) in a blinded fashion.

**Statistical analysis.** Unless stated otherwise, significance was calculated by unpaired, two-sided Student's t-test, \*\*\* P<0.001, \*\*P<0.01, \*P<0.05.

## Results

### 1. Complete loss of RNase H2 in the epidermis results in epithelial hyperproliferation and loss of stem cells

We inactivated the *Rnaseh2b* gene selectively in the epidermis by crossing *Rnaseh2b*<sup>FLOX</sup> mice[23] to the K14-Cre line that deletes loxP-flanked DNA in all basal cells of skin epithelium including hair follicles [23, 33]. *Rnaseh2b*<sup>FL/FL</sup>K14-Cre mice (*Rnaseh2*<sup>EKO</sup> mice) showed strong reduction of *Rnaseh2b* transcripts and RNase H2 activity in total epidermis or FACS-purified epidermal cells, as expected (Fig. S1a, b, c). The animals were conspicuous already few days after birth, showing significant hyperpigmentation, most prominently of ears, snout, tails and paws (Fig.1a), a known sign of ongoing DNA damage responses in mouse epidermis[37, 38]. While whiskers were hypomorphic and reduced in number already in young mice (Fig.1a), the fur initially appeared macroscopically normal. However, *Rnaseh2*<sup>EKO</sup> mice began to loose hair at about 12 weeks and were almost completely nude by 20 weeks (Fig.1a).



Histologically, *Rnaseh2*<sup>EKO</sup> epidermis was normal at the age of 5 weeks except for discrete hyperkeratosis (thickening of the cornified layer). In older animals (10-13 weeks and 18-21 weeks), focal thickening of the epithelium and moderate hyperkeratosis suggested increased epithelial proliferation (Fig.1b). Immunostaining for the cell cycle marker Ki67 (Fig.1b) revealed increased numbers of proliferating epithelial cells in *Rnaseh2*<sup>EKO</sup> compared to control skin in all age groups tested. More rapid proliferation was paralleled by a strong increase in the frequency of apoptotic keratinocytes as detected by staining for active caspase 3 (Fig.1c, d). Loss of hair follicles did not account for the almost complete baldness of *Rnaseh2*<sup>EKO</sup> mice as substantial numbers of follicles were still present even at 30 weeks of age (Fig.S1d). In their active (anagen) phase, hair follicles grow to extend well into the dermal adipose tissue paralleled by thickening of the adipose tissue, whereas resting (telogen) follicles are usually confined to the dermal collagen layer. Numbers of anagen follicles were not different from control numbers at 5 weeks of age. At 10-13 weeks, we found no follicles extending into the adipose layer in control skin, indicating a synchronous resting phase of the hair cycle in this part of the body. In contrast, all *Rnaseh2*<sup>EKO</sup> mice featured numerous 'active' follicles at this time point, demonstrating disturbed hair cycle regulation (Fig.1e). This was also reflected by increased thickness of *Rnaseh2*<sup>EKO</sup> skin at 10-13 weeks as determined by skin fold measurements (Fig.S1e). Loss of hair follicle function in older *Rnaseh2*<sup>EKO</sup> mice suggested exhaustion of epithelial regenerative capacity. In accordance with this notion, we found that the number of hair follicle stem cells, in particular bulge stem cells (CD49<sup>+</sup>CD34<sup>+</sup>Sca1<sup>lo</sup>) was strongly reduced in older mutants compared to controls, as determined by flow cytometric analysis of epidermal single cell suspensions (Fig.1f and S1f). In contrast, other undifferentiated epidermal cell populations were not reduced in mutant skin (Fig.1f and S1f).

Collectively, loss of RNase H2 in the epidermis results in more rapid epithelial cell turnover due to enhanced epithelial cell proliferation and apoptosis, associated with reduction of hair follicle stem cell numbers and loss of hair follicle function.

## **2. Spontaneous type I IFN response and inflammation in *Rnaseh2*<sup>EKO</sup> skin**

Histology and flow cytometry revealed enhanced leukocyte infiltration of *Rnaseh2*<sup>EKO</sup> skin (Fig.2a,b), which was accentuated around hair follicles (Fig.2a). Inflammatory cell invasion into the epithelium was associated with degeneration of the outer-most epithelial cells of the hairfollicle (Fig.2a), an inflammation pattern ('interface dermatitis') typical of skin lesions in SLE [39].

Since RNase H2-deficiency was shown to be associated with spontaneous activation of type I IFN responses [31, 32], we quantified transcript levels of type I IFN-inducible genes (ISGs) in *Rnaseh2*<sup>EKO</sup> and control skin by qRT-PCR analysis. ISG mRNAs were strongly increased

in total epidermis and in purified keratinocytes from young and older mutant mice (Fig.2c, Fig.S2a). Comparison of transcriptomes of leukocytes from control versus *Rnaseh2<sup>EKO</sup>* skin showed upregulation of multiple ISGs in the cells from the mutants, indicating exposure to type I IFN (Fig.2d, Table S1).

Type I IFNs were shown to regulate stem cell function in the hematopoietic system [40]. We therefore addressed what role the chronic IFN response in *Rnaseh2<sup>EKO</sup>* epidermis played and crossed *Rnaseh2<sup>EKO</sup>* mice to a type I IFN receptor knock out (*Ifnar1<sup>-/-</sup>*) line [41] (Fig.S2b). Hyperpigmentation, hair loss (Fig.2e), hyperkeratosis and focal epidermal thickening (Fig.S2c), and inflammatory leukocyte infiltration (Fig.2f) of *Rnaseh2<sup>EKO</sup>* skin were not mitigated by additional inactivation of type I IFN signaling. *Rnaseh2<sup>EKO</sup>Ifnar1<sup>-/-</sup>* mice showed a reduction of hair follicle stem cell numbers compared to controls (Fig.2g), similar to IFNAR-competent *Rnaseh2<sup>EKO</sup>* mice (Fig.1e).

Collectively, the skin inflammation of *Rnaseh2<sup>EKO</sup>* mice is associated with type I IFN production, however, leukocyte infiltration, epidermal hyperproliferation and loss of hair follicle function occur independent of type I IFN.

### **3. Loss of RNase H2 in the epidermis results in spontaneous DNA damage and skin cancer**

Spontaneous DNA damage and activation of DNA damage responses was shown in RNase H2-deficient embryos and cells [12, 23]. Moreover, the hyperpigmented skin of *Rnaseh2<sup>EKO</sup>* mice is suggestive of chronic DNA damage responses in the epidermis [37, 38]. Immunostaining of skin sections for  $\gamma$ H2AX and 53BP1 repair foci indeed revealed increased numbers of  $\gamma$ H2AX and 53BP1 foci in *Rnaseh2<sup>EKO</sup>* compared to control epidermal cells (Fig.3a, Fig.S3a), consistent with increased frequencies of double-strand breaks in RNase H2-deficient yeast [21]. In line with this finding, transcriptome analysis of flow cytometrically purified *Rnaseh2<sup>EKO</sup>* keratinocytes showed up-regulation of several p53-inducible genes compared to control cells (Fig.3b, Table S2), indicating ongoing DNA damage responses.

Starting from week 12, *Rnaseh2<sup>EKO</sup>* mice develop chronic ulcerations of the skin, most frequently in the dorsal neck area, affecting most animals by the age of 1 year (Fig.3c). All *Rnaseh2<sup>EKO</sup>* mice had to be sacrificed between 23 and 55 weeks of age due to these ulcerations, and/or because of large tumors in various locations, often in the mandibular region close to the ear (Fig.3c). Histology revealed (Fig.3d, Table S3) that all ulcerations occurred in neoplastic skin that was classified keratinocyte intraepithelial neoplasia (KIN) [42], i.e. malignant epidermal growth that has not yet breached the epithelial basement membrane, also called 'carcinoma in situ'. In three of these cases, the tumor had focally broken through the basement membrane and was thus classified invasive squamous cell carcinoma (SSC). All macroscopic tumors histologically proved to be invasive SSC, except for two, which were

KIN producing large masses of cornified material (Fig.3d, Table S3). Figure 3e shows that 100% of *Rnaseh2*<sup>EKO</sup> mice developed cancer of at least the KIN stage by about 50 weeks of age. By this time, 60% of the animals had already progressed to invasive SSC (Fig.3e). Additional inactivation of type I IFN signaling resulted in a slight (albeit insignificant) acceleration of neoplastic skin ulceration (Fig.S3b), most likely reflecting loss of stimulation of anti-tumor immunity by type I IFN.

Collectively, we show that RNase H2-deficient hyperproliferative epidermis features spontaneous DNA damage as demonstrated by increased numbers of repair foci and increased transcript levels of p53-inducible genes, and progresses to cancer in 100% of the animals within the first year of life.

#### **4. Additional loss of p53 in *Rnaseh2*<sup>EKO</sup> mice enhances the epidermal IFN response and accelerates hyperproliferation and carcinogenesis**

In order to determine the effect of p53-dependent DNA damage responses on the *Rnaseh2*<sup>EKO</sup> phenotype, we crossed *Rnaseh2*<sup>EKO</sup> to *Trp53*<sup>-/-</sup> mice [34] and observed potent effects of *Trp53* gene dose. *Rnaseh2*<sup>EKO</sup> mice heterozygous for the *Trp53*<sup>null</sup> allele showed ameliorated hyperpigmentation compared to p53-competent controls (Fig.S4a) and no sign of alopecia until the age of 40 weeks. All *Rnaseh2*<sup>EKO</sup> *Trp53*<sup>+/-</sup> mice that were allowed to age had to be sacrificed because of macroscopic ulcerations or skin tumors before the age of 40 weeks. Histology showed that these lesions were invasive SSC of various stages and grades (Table S4, Fig.4a).

Biallelic loss of *Trp53* completely reverted the hyperpigmentation of *Rnaseh2*<sup>EKO</sup> (Fig.4b, Fig.S4a). While no generalized alopecia was observed, all of these animals developed inflamed lesions associated with circumscribed loss of hair and extensive scratching in the neck area, starting at about 12 weeks of age (Fig.4b). Massive pruritus and erosions of the neck skin invariably required euthanasia few weeks later. In all cases, histology identified KIN of different stages as the cause of the lesions (Fig.4c, Tables S5 and S6). Ki67 immunostaining showed the massive proliferation of cells in all strata of the epithelium typical of KIN (Fig.4d). Inactivation of p53 signaling resulted in survival of more cells with a higher damage load as demonstrated by immunostaining for  $\gamma$ H2AX repair foci (Fig.4e, Fig.S4b) as compared to p53 competent *Rnaseh2*<sup>EKO</sup> skin (Fig.3a). Flow cytometric analysis of *Rnaseh2*<sup>EKO</sup>*Trp53*<sup>-/-</sup> skin revealed that the loss of hair follicle stem cells caused by epidermal RNase H2 deficiency was prevented by lack of p53. Interestingly, hair follicle stem cell numbers of *Rnaseh2*<sup>EKO</sup>*Trp53*<sup>-/-</sup> epidermis ranged about 3-fold higher compared to control numbers (Fig.4f).

Compared to p53-competent *Rnaseh2*<sup>EKO</sup> mice, leukocyte infiltration was more pronounced in *Rnaseh2*<sup>EKO</sup>*Trp53*<sup>-/-</sup> skin (Fig.S4c). A potential reason for enhanced skin inflammation of

these animals might be potentiated cytokine responses as we found strongly increased ISG mRNA levels in total epidermis and in keratinocytes of *Trp53*<sup>-/-</sup> as compared to p53-proficient *Rnaseh2*<sup>EKO</sup> mice (Fig.4g), demonstrating that p53-dependent DNA damage responses control the intensity of the STING-induced IFN response mounted by RNase H2-deficient keratinocytes. While we have shown that type I IFN was not causing the inflammation of *Rnaseh2*<sup>EKO</sup> skin (Fig.2f), STING-mediated, NFκB-dependent proinflammatory cytokine expression, triggered in parallel to the IFN response, could be responsible for the enhanced inflammation of IFNAR-deficient *Rnaseh2*<sup>EKO</sup> skin.

In summary, cancer development in *Rnaseh2*<sup>EKO</sup> mice is accelerated by additional absence of p53. This finding demonstrates that p53-dependent elimination of epithelial cells with high damage load potentially antagonizes oncogenic transformation of RNase H2-deficient epidermis.

## Discussion

DNA polymerases do not replicate genomic DNA without mistakes. They incorporate nucleotides carrying the wrong base or wrong sugar at substantial rates. In order to ensure genome integrity, two DNA repair pathways operate on the newly synthesized strand to correct these replication errors. MMR, which removes nucleotides that do not base-pair correctly with the template strand, and RER, which removes ribonucleotides, that are incorporated into the genomic DNA at a rate of 1 every 7,600 nucleotides [12] and threaten genome stability. Humans and mice with genetic defects causing loss of mismatch repair activity are viable but exhibit strongly increased cancer risk [6, 7, 43]. Genetic defects of RER leading to inability to remove ribonucleotides from genomic DNA result in embryonic lethality in the mouse [12, 23] and most likely also in humans, as partial loss of function mutations of the genes encoding RNase H2, the enzyme essential for initiation of RER, can result in severe disease and biallelic complete null alleles have not been found [44].

We bypassed embryonic lethality of global RER deficiency by conditional inactivation of the *Rnaseh2b* gene only in the epidermis of the skin and observed spontaneous DNA damage and epithelial hyperproliferation, resulting in spontaneous cancer development in 100% of the animals within the first year of life. Thus, we showed that RER is essential to prevent malignant transformation.

While the epithelium proliferated rapidly, it featured a high rate of keratinocyte apoptosis induced by p53 activation. Cancer development driven by epidermal RER deficiency was accelerated upon additional loss of one allele of the *Trp53* gene. In *Rnaseh2*<sup>EKO</sup> mice harboring two *Trp53* null alleles, the skin of neck and back transformed into one large confluent carcinoma in situ between 10 and 20 weeks of age. It seems likely that this process would have affected the entire skin and would have rapidly progressed to invasive SSC with

increasing age, if not for the fact that the animals had to be euthanized for severe itch and erosions.

Carcinogenesis triggered by defective RNase H2 seems to require reduction of RNase H2 activity to low levels. Mice in which RNase H2 activity was reduced to 30% of control levels due to a homozygous *Rnaseh2b* partial loss-of-function mutation showed spontaneous activation of type I IFN responses but no sign of cancer by the age of 1 year [32]. Likewise, mice that carried a biallelic knock in of a *Rnaseh2a* partial loss-of-function mutation, reducing RNase H2 activity to few percent of normal levels, and that were rescued from perinatal lethality by additional inactivation of STING were not reported to develop neoplastic disease [31]. However, investigation of cancer incidence in a larger cohort of older animals was hampered by the fact that only a small fraction of these mice survived into adulthood [31].

We observed accelerated proliferation of *Rnaseh2<sup>EKO</sup>* epidermis, resulting in epidermal hyperplasia and thickening of the cornified layer (hyperkeratosis) despite greatly increased rates of keratinocyte apoptosis. An important inducer of apoptosis in *Rnaseh2<sup>EKO</sup>* skin was p53, since additional loss of p53 resulted in significant further acceleration of epithelial hyperproliferation. These rapid cell divisions in response to keratinocyte genome damage ensuing from RER deficiency likely reflect a response program that the epidermis executes upon exposure to multiple forms of DNA damage, aiming at improved light protection by increasing thickness of epidermis and cornified layer, associated with enhanced melanin production, as we also observed in our animals. This response is activated for example upon over-exposure to UV irradiation [45]. Enhanced epidermal proliferation upon genome damage also results in elimination of damaged cells through rapid epithelial turnover, which represents an alternative keratinocyte disposal pathway in addition to apoptosis [46]. Damaged basal cells arrest in late S-phase, detach from the basement membrane and get eliminated into the cornified layer [46].

Accelerated epithelial turnover in *Rnaseh2<sup>EKO</sup>* skin was associated with disturbed hair cycle regulation with progressive loss of hair follicle stem cells and hair follicle function. This might be a result of exhaustion of this stem cell population due to increased demand for differentiated keratinocytes, but may also reflect loss of hair follicle stem cells through apoptosis or terminal differentiation and transepidermal elimination. The latter was described to be the major cause for physiological hair follicle aging and for premature hair follicle deterioration enforced by ionizing irradiation or genetic defects of nucleotide excision repair [47]. Other epidermal stem cell populations were not reduced in numbers, likely reflecting differential responses to genome damage caused by defective RER. Specific responses of different stem cell populations to genome damage are documented in various tissues [48]. Hair follicle stem cells were found to be more resistant to cell death induction by ionizing irradiation compared to other epidermal stem cell populations due to their capability to rapidly

repair double strand breaks by non-homologous end joining and high level expression of the anti-apoptotic protein Bcl2 [49]. Epidermis-specific inactivation of homologous recombination repair by conditional knock out of BRCA1, however, resulted in selective depletion of hair follicle stem cells [50], similar to the loss of hair follicle stem cells in our *Rnaseh2<sup>EKO</sup>* animals. In both mouse lines, loss of hair and hair follicle stem cells are largely rescued by additional inactivation of the *Trp53* gene [50], indicating p53-dependent cell death induction by RER deficiency in these cells. Additional absence of p53 in *Rnaseh2<sup>EKO</sup>* mice not only restored stem cell numbers to control levels, but resulted in three-fold higher hair follicle stem cell numbers compared to RER competent controls, likely reflecting pre-neoplastic expansion of this population.

Rapid progression to cancer in 100% of the animals with epidermis-specific loss of RER activity, even despite intact p53 signaling, raises the question of whether mutations impairing RER are relevant for human cancer. However, the studies of cancer incidence in AGS patients carrying defects of *RNASEH2* genes are hampered by their reduced life span [51].

Germline mutations compromising RER as well as somatic defects of RER acquired by growing tumor clones could affect tumor biology in two opposite ways. On one hand, DNA damage ensuing from unrepaired ribonucleotides causes genomic instability, thus promoting carcinogenesis and tumor progression. On the other hand, high rates of tumor cell death or senescence induction by persistent DNA lesions will antagonize malignant growth and can confer a competitive disadvantage to tumor cells. The net effect, tumor promotion or suppression, likely depends on the degree to which RER activity is reduced. A window of low RER activity advantageous for tumor growth may exist. The net effect of RER deficiency on cancer biology likely also depends on tumor type, as different cell types and cells of the same type but different differentiation stage show specific responses to DNA damage ranging from apoptosis and senescence to enforced differentiation [48, 52]. In addition to detection of damage by nuclear sensors likely occurring in RNase H2-deficient cells, micronucleus formation associated with RER deficiency and subsequent micronuclear envelope rupture were shown to lead to frequent exposure of chromosomal DNA to the cytosolic DNA sensor cGAS, resulting in the activation of STING [24]. STING is also activated upon DNA damage by herniation of chromatin into the cytosol [26]. The potent type I IFN response we observed in *Rnaseh2<sup>EKO</sup>* skin most likely reflects activation of the cGAS-STING axis. Potentiation of this IFN response in the absence of functional p53 strongly suggests that genome damage is responsible for STING activation in our animals, as lack of p53 allows cells with high damage load producing IFN to survive longer. STING can trigger differential responses, including senescence or apoptosis as well as antiviral and inflammatory cytokine production stimulating immune activation, depending on signal strength and cell type. RER-deficient epidermis invariably develops cancer despite robust

STING activation and production of type IFN, which can strongly boost anti-tumor immunity [53]. Intriguingly, STING-mediated innate immune responses can also promote neoplastic growth, as STING activation by micronuclear DNA in chromosomally unstable cancer cells was recently shown to drive metastasis by activation of non-canonical NF- $\kappa$ B signaling [54]. Assessing contributions of RER defects to human cancer requires studies correlating frequencies of partial loss-of-function mutations in *RNASEH2* genes, either in the germ-line or the tumor tissue of the patients, in particular cancer entities. Increased frequencies of RNASEH2B partial loss-of-function mutations were found in the germline of sporadic prostate cancer patients compared to control cohorts [55]. RNASEH2B partial loss-of-function mutations were also detected at higher frequencies in non-tumor DNA of glioma patients with familial cancer predisposition and co-segregated with manifestation of cancer in some of the families [55]. These findings provide first hints that compromised RER activity can be associated with human cancer.

### **Acknowledgements**

We thank Tobias Häring for expert technical assistance.

The study was supported by grant 2015\_A100 of the Else Kröner-Fresenius Foundation to A. Roers and R. Behrendt, by German Research Foundation (DFG) grant Ro2133/6-1 in the setting of Clinical Research Unit KFO249 to A. Roers. R. Behrendt is supported by the Aicardi-Goutières Syndrome Americas Association. Work in the laboratory of A.P. Jackson was supported by the Medical Research Council (MRC, U127580972).

## References

1. Hoeijmakers, J.H., *DNA damage, aging, and cancer*. N Engl J Med, 2009. **361**(15): p. 1475-85.
2. Lindahl, T. and R.D. Wood, *Quality control by DNA repair*. Science, 1999. **286**(5446): p. 1897-905.
3. Ganai, R.A. and E. Johansson, *DNA Replication-A Matter of Fidelity*. Mol Cell, 2016. **62**(5): p. 745-55.
4. Kunkel, T.A., *Evolving views of DNA replication (in)fidelity*. Cold Spring Harb Symp Quant Biol, 2009. **74**: p. 91-101.
5. Kunkel, T.A. and D.A. Erie, *Eukaryotic Mismatch Repair in Relation to DNA Replication*. Annu Rev Genet, 2015. **49**: p. 291-313.
6. Lynch, H.T., et al., *Milestones of Lynch syndrome: 1895-2015*. Nat Rev Cancer, 2015. **15**(3): p. 181-94.
7. Wimmer, K. and J. Etzler, *Constitutional mismatch repair-deficiency syndrome: have we so far seen only the tip of an iceberg?* Hum Genet, 2008. **124**(2): p. 105-22.
8. Nick McElhinny, S.A., et al., *Abundant ribonucleotide incorporation into DNA by yeast replicative polymerases*. Proc Natl Acad Sci U S A, 2010. **107**(11): p. 4949-54.
9. Joyce, C.M., *Choosing the right sugar: how polymerases select a nucleotide substrate*. Proc Natl Acad Sci U S A, 1997. **94**(5): p. 1619-22.
10. Nick McElhinny, S.A., et al., *Genome instability due to ribonucleotide incorporation into DNA*. Nat Chem Biol, 2010. **6**(10): p. 774-81.
11. Traut, T.W., *Physiological concentrations of purines and pyrimidines*. Mol Cell Biochem, 1994. **140**(1): p. 1-22.
12. Reijns, M.A., et al., *Enzymatic removal of ribonucleotides from DNA is essential for mammalian genome integrity and development*. Cell, 2012. **149**(5): p. 1008-22.
13. Williams, J.S., S.A. Lujan, and T.A. Kunkel, *Processing ribonucleotides incorporated during eukaryotic DNA replication*. Nat Rev Mol Cell Biol, 2016. **17**(6): p. 350-63.
14. Sparks, J.L., et al., *RNase H2-initiated ribonucleotide excision repair*. Mol Cell, 2012. **47**(6): p. 980-6.
15. Cerritelli, S.M. and R.J. Crouch, *The Balancing Act of Ribonucleotides in DNA*. Trends Biochem Sci, 2016. **41**(5): p. 434-45.
16. Lujan, S.A., et al., *Ribonucleotides are signals for mismatch repair of leading-strand replication errors*. Mol Cell, 2013. **50**(3): p. 437-43.
17. Ghodgaonkar, M.M., et al., *Ribonucleotides misincorporated into DNA act as strand-discrimination signals in eukaryotic mismatch repair*. Mol Cell, 2013. **50**(3): p. 323-32.
18. Williams, J.S., et al., *Evidence that processing of ribonucleotides in DNA by topoisomerase 1 is leading-strand specific*. Nat Struct Mol Biol, 2015. **22**(4): p. 291-7.
19. Caldecott, K.W., *Molecular biology. Ribose--an internal threat to DNA*. Science, 2014. **343**(6168): p. 260-1.
20. Kim, N., et al., *Mutagenic processing of ribonucleotides in DNA by yeast topoisomerase I*. Science, 2011. **332**(6037): p. 1561-4.
21. Huang, S.N., et al., *Topoisomerase I-mediated cleavage at unrepaired ribonucleotides generates DNA double-strand breaks*. EMBO J, 2017. **36**(3): p. 361-373.
22. Chon, H., et al., *RNase H2 roles in genome integrity revealed by unlinking its activities*. Nucleic Acids Res, 2013. **41**(5): p. 3130-43.
23. Hiller, B., et al., *Mammalian RNase H2 removes ribonucleotides from DNA to maintain genome integrity*. J Exp Med, 2012. **209**(8): p. 1419-26.
24. Mackenzie, K.J., et al., *cGAS surveillance of micronuclei links genome instability to innate immunity*. Nature, 2017. **548**(7668): p. 461-465.
25. Bartsch, K., et al., *Absence of RNase H2 triggers generation of immunogenic micronuclei removed by autophagy*. Hum Mol Genet, 2017. **26**(20): p. 3960-3972.
26. Gluck, S., et al., *Innate immune sensing of cytosolic chromatin fragments through cGAS promotes senescence*. Nat Cell Biol, 2017. **19**(9): p. 1061-1070.



27. Crow, Y.J., et al., *Mutations in genes encoding ribonuclease H2 subunits cause Aicardi-Goutieres syndrome and mimic congenital viral brain infection*. Nat Genet, 2006. **38**(8): p. 910-6.
28. Crow, Y.J. and N. Manel, *Aicardi-Goutieres syndrome and the type I interferonopathies*. Nat Rev Immunol, 2015. **15**(7): p. 429-40.
29. Reijns, M.A., et al., *The structure of the human RNase H2 complex defines key interaction interfaces relevant to enzyme function and human disease*. J Biol Chem, 2011. **286**(12): p. 10530-9.
30. Chon, H., et al., *Contributions of the two accessory subunits, RNASEH2B and RNASEH2C, to the activity and properties of the human RNase H2 complex*. Nucleic Acids Res, 2009. **37**(1): p. 96-110.
31. Pokatayev, V., et al., *RNase H2 catalytic core Aicardi-Goutieres syndrome-related mutant invokes cGAS-STING innate immune-sensing pathway in mice*. J Exp Med, 2016. **213**(3): p. 329-36.
32. Mackenzie, K.J., et al., *Ribonuclease H2 mutations induce a cGAS/STING-dependent innate immune response*. EMBO J, 2016. **35**(8): p. 831-44.
33. Hafner, M., et al., *Keratin 14 Cre transgenic mice authenticate keratin 14 as an oocyte-expressed protein*. Genesis, 2004. **38**(4): p. 176-81.
34. Jacks, T., et al., *Tumor spectrum analysis in p53-mutant mice*. Curr Biol, 1994. **4**(1): p. 1-7.
35. Jensen, K.B., R.R. Driskell, and F.M. Watt, *Assaying proliferation and differentiation capacity of stem cells using disaggregated adult mouse epidermis*. Nat Protoc, 2010. **5**(5): p. 898-911.
36. Love, M.I., W. Huber, and S. Anders, *Moderated estimation of fold change and dispersion for RNA-seq data with DESeq2*. Genome Biol, 2014. **15**(12): p. 550.
37. Chang, C.H., et al., *CK1alpha ablation in keratinocytes induces p53-dependent, sunburn-protective skin hyperpigmentation*. Proc Natl Acad Sci U S A, 2017. **114**(38): p. E8035-E8044.
38. Cui, R., et al., *Central role of p53 in the suntan response and pathologic hyperpigmentation*. Cell, 2007. **128**(5): p. 853-64.
39. Wenzel, J. and T. Tuting, *An IFN-associated cytotoxic cellular immune response against viral, self-, or tumor antigens is a common pathogenetic feature in "interface dermatitis"*. J Invest Dermatol, 2008. **128**(10): p. 2392-402.
40. Essers, M.A., et al., *IFNalpha activates dormant haematopoietic stem cells in vivo*. Nature, 2009. **458**(7240): p. 904-8.
41. Kamphuis, E., et al., *Type I interferons directly regulate lymphocyte recirculation and cause transient blood lymphopenia*. Blood, 2006. **108**(10): p. 3253-61.
42. Fernandez Figueras, M.T., *From actinic keratosis to squamous cell carcinoma: pathophysiology revisited*. J Eur Acad Dermatol Venereol, 2017. **31 Suppl 2**: p. 5-7.
43. Lee, K., E. Tosti, and W. Edlmann, *Mouse models of DNA mismatch repair in cancer research*. DNA Repair (Amst), 2016. **38**: p. 140-6.
44. Rice, G., et al., *Clinical and molecular phenotype of Aicardi-Goutieres syndrome*. Am J Hum Genet, 2007. **81**(4): p. 713-25.
45. Sterenborg, H.J., F.R. de Gruijl, and J.C. van der Leun, *UV-induced epidermal hyperplasia in hairless mice*. Photodermatol, 1986. **3**(4): p. 206-14.
46. Stout, G.J., et al., *Epidermal transit of replication-arrested, undifferentiated keratinocytes in UV-exposed XPC mice: an alternative to in situ apoptosis*. Proc Natl Acad Sci U S A, 2005. **102**(52): p. 18980-5.
47. Matsumura, H., et al., *Hair follicle aging is driven by transepidermal elimination of stem cells via COL17A1 proteolysis*. Science, 2016. **351**(6273): p. aad4395.
48. Blanpain, C., et al., *DNA-damage response in tissue-specific and cancer stem cells*. Cell Stem Cell, 2011. **8**(1): p. 16-29.
49. Sotiropoulou, P.A., et al., *Bcl-2 and accelerated DNA repair mediates resistance of hair follicle bulge stem cells to DNA-damage-induced cell death*. Nat Cell Biol, 2010. **12**(6): p. 572-82.

50. Sotiropoulou, P.A., et al., *BRCA1 deficiency in skin epidermis leads to selective loss of hair follicle stem cells and their progeny*. Genes Dev, 2013. **27**(1): p. 39-51.
51. Crow, Y.J., et al., *Characterization of human disease phenotypes associated with mutations in TREX1, RNASEH2A, RNASEH2B, RNASEH2C, SAMHD1, ADAR, and IFIH1*. Am J Med Genet A, 2015. **167A**(2): p. 296-312.
52. Lans, H. and W. Vermeulen, *Tissue specific response to DNA damage: C. elegans as role model*. DNA Repair (Amst), 2015. **32**: p. 141-8.
53. Zitvogel, L., et al., *Type I interferons in anticancer immunity*. Nat Rev Immunol, 2015. **15**(7): p. 405-14.
54. Bakhoum, S.F., et al., *Chromosomal instability drives metastasis through a cytosolic DNA response*. Nature, 2018. **553**(7689): p. 467-472.
55. Beyer, U., et al., *Rare ADAR and RNASEH2B variants and a type I interferon signature in glioma and prostate carcinoma risk and tumorigenesis*. Acta Neuropathol, 2017. **134**(6): p. 905-922.

## Figure Legends

**Figure 1.** Epithelial hyperproliferation and stem cell exhaustion in mice lacking RNase H2 in the epidermis (*Rnaseh2<sup>EKO</sup>*)

**a)** Macroscopic phenotype of 15 week-old *Rnaseh2<sup>EKO</sup>* mouse and a control (*Rnaseh2b<sup>FL/FL</sup>Cre-negative*) littermate.

**b)** Representative histology of back skin from a 12 week-old *Rnaseh2<sup>EKO</sup>* and a control (*Rnaseh2b<sup>FL/FL</sup>Cre-negative*) littermate. Left: hematoxylin-eosin (H&E) staining showing focal epithelial thickening and hyperkeratosis (thickening of cornified layer) of mutant epidermis (see supplementary material for detailed histopathological findings); right: Ki67 immunostaining showing increased proliferation of mutant epidermis. Scale bars 40µm. Graph shows numbers of Ki67<sup>+</sup> interfollicular epidermal cells per high power field (40x); mean ± SD, \*p=0.014 (5 weeks), \*\*p=0.0039 (10-12 weeks), \*\*\*p=0.0007 (18-21 weeks), \*p=0.0101 (30 weeks).

**c)** Detection of apoptotic cells in interfollicular epidermis by immunostaining for active caspase 3 in back skin sections of *Rnaseh2<sup>EKO</sup>* mice and control (*Rnaseh2b<sup>FL/FL</sup>Cre-negative*) littermates. Representative images are shown. Scale bar 50 µm.

**d)** Quantification of active caspase 3 per mm epidermal length (n=6-10 per group and time point); means ± SD, \*\*p=0.0073 (10-13 weeks), \*\*\*p<0.0001 (18-21 weeks).

**e)** Quantification of 'active' hair follicles (i.e. follicles extending beyond the dermal collagen into the dermal adipose layer, thus including follicles in anagen II-VI and early catagen stages) per low power (10x) field in H&E stained back skin sections of *Rnaseh2<sup>EKO</sup>* mice and control (*Rnaseh2b<sup>FL/FL</sup>Cre-negative*) littermates; means ± SD, \*p=0.0391 (10-13 weeks), \*p=0.0335 (18-21 weeks).

**f)** Flow cytometric quantification of epithelial stem cell populations in back skin of *Rnaseh2<sup>EKO</sup>* mice and control (*Rnaseh2b<sup>FL/FL</sup>Cre-negative*) littermates. See Fig.S1 for gating. SCs, stem cells; HFSC, hair follicle stem cells; IFE, interfollicular epidermis; mean and SD, \*\*p=0.0011 (suprabasal bulge SCs, 20 weeks), \*p=0.0205 (bulge SCs, 10-12 weeks), \*\*p=0.0033 (bulge SCs, 20 weeks), \*p=0.0239 (IFE+ infundibulum SCs, 20 weeks).

**Figure 2.** Loss of RNase H2 in the epidermis results in spontaneous type I IFN response and inflammation

**a)** Representative *Rnaseh2<sup>EKO</sup>* back skin section (age 10-12 weeks) immunostained for CD45 (purple) for identification of hematopoietic cells (see supplementary material for detailed histopathological findings). Original magnification x200.

**b)** Quantification of CD45<sup>+</sup> leukocytes in single cell suspensions prepared from the epidermal compartment of back skin from 10-12 week-old *Rnaseh2<sup>EKO</sup>* (*EKO*) mice (n=10) and control (*Rnaseh2b<sup>FL/FL</sup>Cre-negative*) littermates (n=9). Mean and SD, \*\*\*p<0.0001.

**c)** Comparison of ISG transcript levels determined by qRT-PCR in RNA extracted from total epidermis of 10-12 and 20 week-old *Rnaseh2<sup>EKO</sup>* (*EKO*) mice to the mean obtained for control (*Rnaseh2b<sup>FL/FL</sup>Cre-negative*) littermates (10-12 wk n=6, 20 wk n=3) which was set to 1 (dotted line). 10-12 weeks: \*\*p=0.0018 (*Oas1*), \*p=0.0105 (*Ifi44*), \*p=0.0162 (*Viperin*), 20 weeks: \*p=0.0242 (*Oas1*), \*\*p=0.0061 (*Ifi44*), \*p=0.0246 (*Viperin*).

**d)** Comparison of gene expression profiles of FACS-purified CD45<sup>+</sup> leukocytes from epidermis of 12 week-old *Rnaseh2<sup>EKO</sup>* (*EKO*) mice (n=7) and control (*Rnaseh2b<sup>FL/FL</sup>Cre-negative*) littermates (n=6) based on RNA sequencing. Significantly (p<0.05) deregulated genes in black. Significantly deregulated ISGs in red.

**e)** Macroscopic phenotype of an 11 week-old *Ifnar1<sup>-/-</sup>Rnaseh2<sup>EKO</sup>* mouse (note hyperpigmentation of ears, tail and paws, and almost complete hair loss) and a control (*Ifnar1<sup>-/-</sup>Rnaseh2b<sup>FL/FL</sup>Cre-negative*) littermate.

**f)** Quantification of CD45<sup>+</sup> leukocytes in the epidermis of 10-12 week-old *Ifnar1<sup>-/-</sup>Rnaseh2<sup>EKO</sup>* (*EKO*) mice (n=7) and control (*Rnaseh2b<sup>FL/FL</sup>Cre-negative*) littermates (n=7). Mean and SD, \*\*\*p=0.0009.

**g)** Flow cytometric quantification of hair follicle stem cell populations in back skin of 10-12 week-old *Ifnar1<sup>-/-</sup>Rnaseh2<sup>EKO</sup>* mice (n=7) and control (*Ifnar1<sup>-/-</sup>Rnaseh2b<sup>FL/FL</sup>Cre-negative*) littermates (n=7). See Fig.S1f for gating; mean and SD, \*\*\*p<0.0001, \*p=0.0209.

**Figure 3.** Loss of RNase H2 in the epidermis results in spontaneous DNA damage and skin cancer

**a)** Immunostaining of  $\gamma$ H2AX repair foci (green) in back skin of 10-13 week-old *Rnaseh2*<sup>EKO</sup> (EKO) mice (n=7) and control (*Rnaseh2b*<sup>FL/FL</sup>Cre-negative) littermates (n=6). Left: Representative result for EKO and control (DAPI counterstaining). Scale bars 5  $\mu$ m. Right: Quantification of  $\gamma$ H2AX foci per nucleus. At least 220 nuclei (interfollicular epidermis) were counted per animal. Mean and SD, \*\*\*p<0.0001 (one-way ANOVA).

**b)** Comparison of gene expression profiles of FACS-purified keratinocytes from epidermis of 9-12 week-old *Rnaseh2*<sup>EKO</sup> (EKO) mice (n=3) and control (*Rnaseh2b*<sup>FL/FL</sup>Cre-negative) littermates (n=3) based on RNA sequencing. Significantly (p<0.05) deregulated genes in black. Significantly deregulated p53-inducible genes in red.

**c)** Incidence of macroscopic lesions (ulcerations and tumors) in *Rnaseh2*<sup>EKO</sup> mice. Graph indicates the time points at which euthanasia was required for these lesions.

**d)** Representative histology of the lesions represented in c). Upper panels, H&E-stained section of *Rnaseh2*<sup>EKO</sup> skin adjacent to ulceration showing characteristic features of keratinocyte intraepithelial neoplasia (KIN, i.e. cancer that has not yet broken through the basement membrane); scale bars 200  $\mu$ m left, 100  $\mu$ m right. Ki67 immunostaining (lower right) demonstrates proliferating Ki67<sup>+</sup> cells in all strata of the epithelium as is characteristic of KIN; scale bar 40 $\mu$ m. Macroscopic tumor in the genital area of a 36 week-old *Rnaseh2*<sup>EKO</sup> mouse histologically (lower left) proved to be invasive SSC (table S3, animal 62166); scale bar 200  $\mu$ m. See supplementary material for detailed histopathological findings.

**e)** Incidence of invasive SSC and incidence of cancer of all stages (KIN and/or SSC) in *Rnaseh2*<sup>EKO</sup> mice. \*p=0.0131 (log-rank test).

**Figure 4.** Additional loss of p53 in *Rnaseh2<sup>EKO</sup>* mice enhances the epidermal IFN response and accelerates hyperproliferation and cancerogenesis.

**a)** Incidence of invasive SSC (left) and of cancer of all stages (KIN and/or SSC, right) in *Rnaseh2<sup>EKO</sup>* mice that were *Trp53<sup>WT/-</sup>* or *Trp53<sup>-/-</sup>*. Cancer incidence of *Trp53<sup>WT/WT</sup> Rnaseh2<sup>EKO</sup>* mice from Fig.3e shown in light grey for comparison. \*\*\**p*<0.0001 both (log-rank test).

**b)** Macroscopic phenotype of a 10 week-old *Trp53<sup>-/-</sup>Rnaseh2<sup>EKO</sup>* mouse and an 11 week-old control (*Trp53<sup>-/-</sup>Rnaseh2b<sup>FL/FL</sup>Cre-negative*). Note normal pigmentation (tail and paws) of the mutant, in contrast to *Trp53<sup>wtwt</sup>Rnaseh2<sup>EKO</sup>* mice (Fig.1a). Except for an inflamed, hyperkeratotic lesion in the neck with circumscribed hair loss, the fur is largely normal.

**c)** Representative H&E-stained neck skin section of a *Trp53<sup>-/-</sup>Rnaseh2<sup>EKO</sup>* mouse sacrificed for severe itching and erosions. Note typical features of KIN, including massive thickening of epidermis and severe dysplasia of the epithelium (irregular nuclear shape, numerous mitotic figures also in upper strata). See supplementary material for detailed histopathological findings. Scale bar left panel 50  $\mu$ m, inset 20  $\mu$ m.

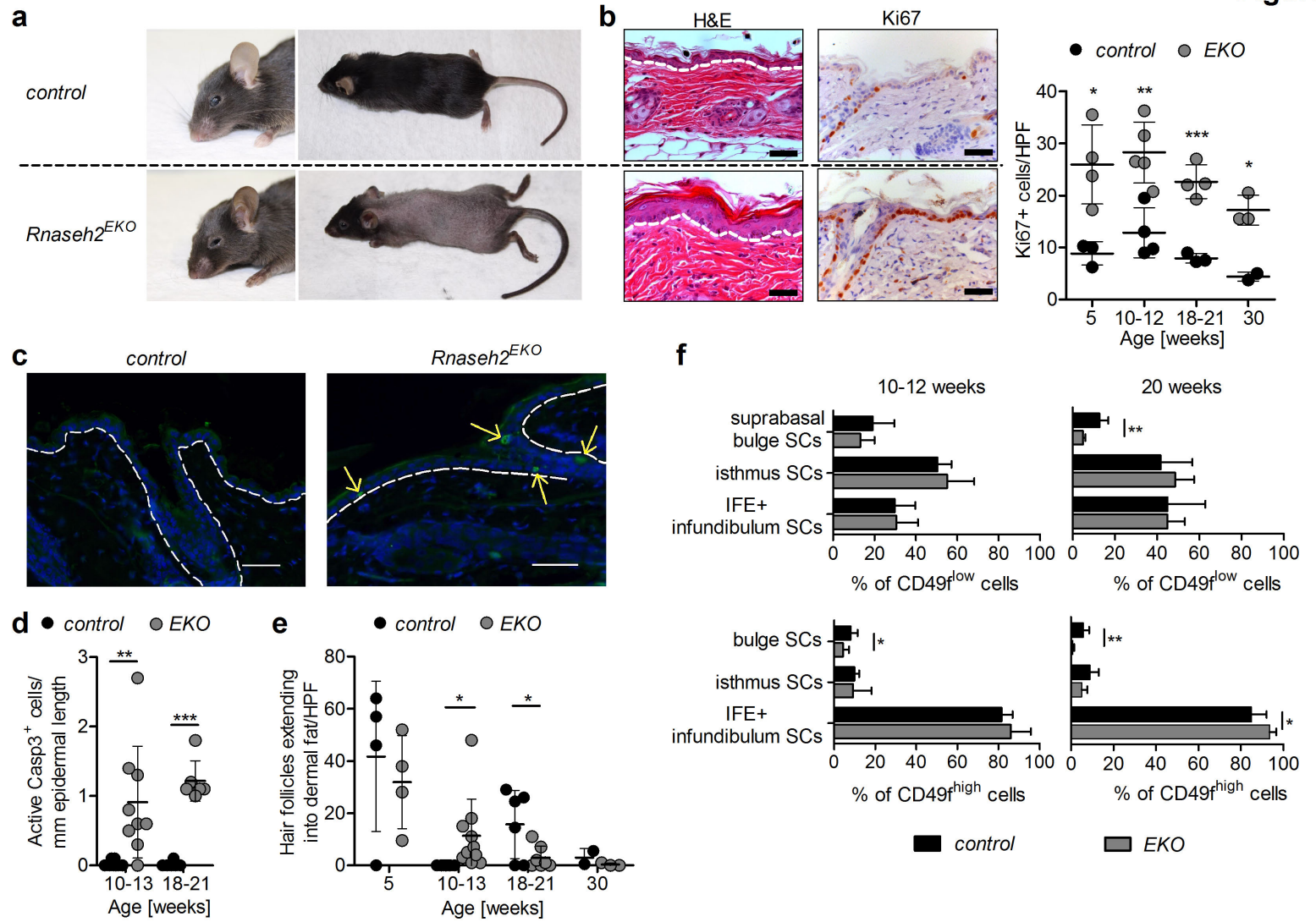
**d)** Immunostaining of neck skin sections of 10-12 week-old *Trp53<sup>-/-</sup>Rnaseh2<sup>EKO</sup>* mice (n=4) and control (*Trp53<sup>-/-</sup>Rnaseh2b<sup>FL/FL</sup>Cre-negative*) littermates (n=8) for Ki67. Representative image of *Trp53<sup>-/-</sup>Rnaseh2<sup>EKO</sup>* skin. Scale bar 50  $\mu$ m. Graph shows numbers of Ki67<sup>+</sup> epidermal cells per randomly placed high power (40x) field. Mean and SD, \*\*\**p*<0.0001.

**e)** Quantification of  $\gamma$ H2AX repair foci in immunostained back skin of 10-13 week-old *p53<sup>-/-</sup>Rnaseh2<sup>EKO</sup>* (EKO) mice (n=4) and control (*Trp53<sup>-/-</sup>Rnaseh2b<sup>FL/FL</sup>Cre-negative*) littermates (n=4). Number of foci was counted in at least 220 nuclei (interfollicular epidermis and follicles) per animal. See Fig.S4b for images. Mean and SD, \*\*\**p*<0.0001 (one-way ANOVA).

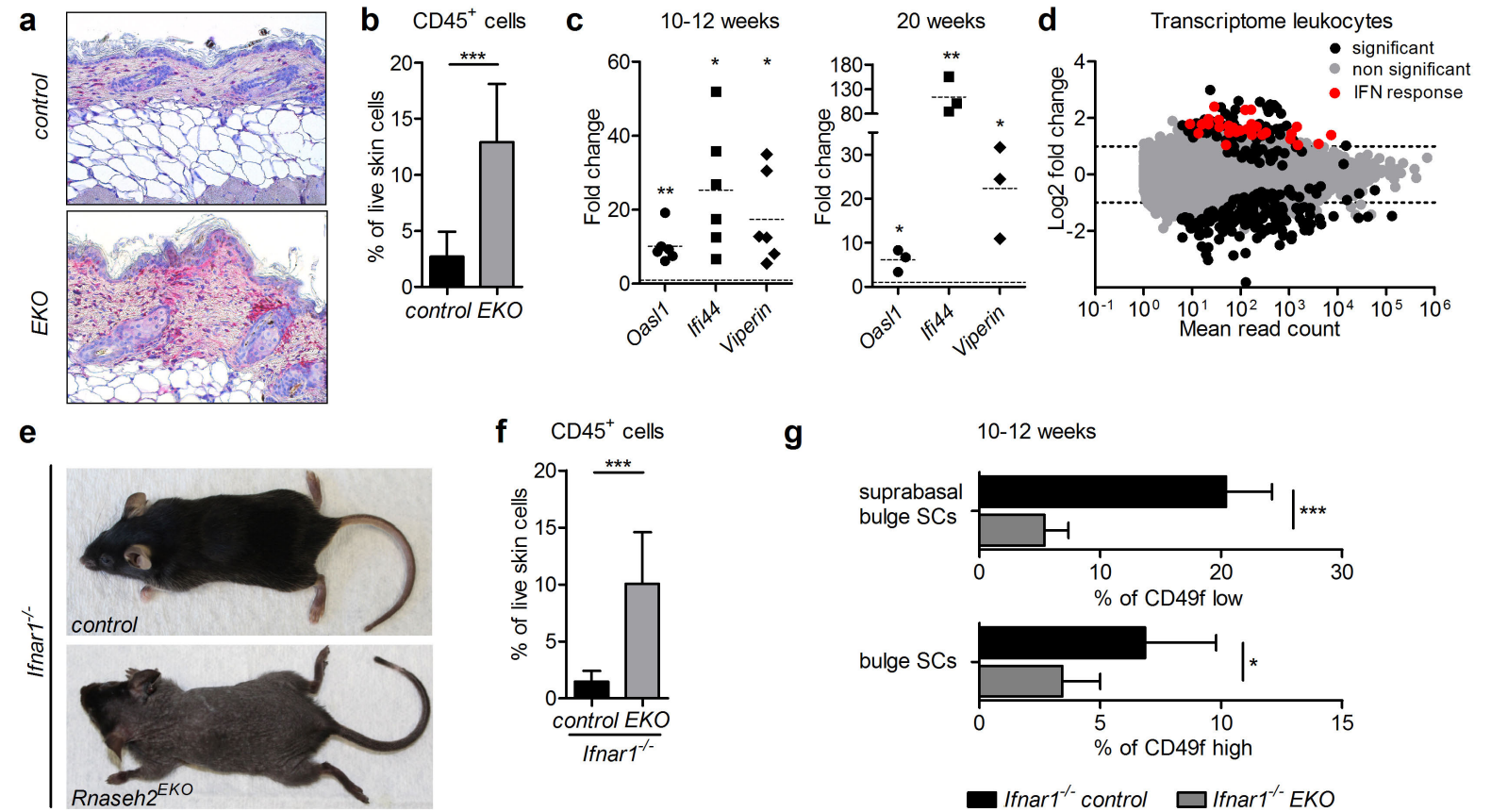
**f)** Flow cytometric quantification of epithelial stem cell populations in back skin of 10-12 week-old *Trp53<sup>-/-</sup>Rnaseh2<sup>EKO</sup>* mice (n=6) and control (*Trp53<sup>-/-</sup>Rnaseh2b<sup>FL/FL</sup>Cre-negative*) littermates (n=5). See Fig.S1f for gating; mean and SD, \*\*\**p*=0.0001.

**g)** Comparison of ISG transcript levels determined by qRT-PCR in RNA extracted from total epidermis (left) or FACS-purified keratinocytes (right) of 10-12 week-old *Trp53<sup>+/-</sup>Rnaseh2<sup>EKO</sup>* and *Trp53<sup>-/-</sup>Rnaseh2<sup>EKO</sup>* mice to the mean obtained for the respective control group, which was set to 1. left: \*\*\**p*=0.0005 (*Oas1*), \*\*\**p*<0.0001 (*Ifi44*), \*\**p*=0.0066 (*Viperin*), right: \*\**p*=0.0042 (*Oas1*). (p53 deficiency alone did not cause a spontaneous IFN response, see Fig.S4d.)

**Figure 1**

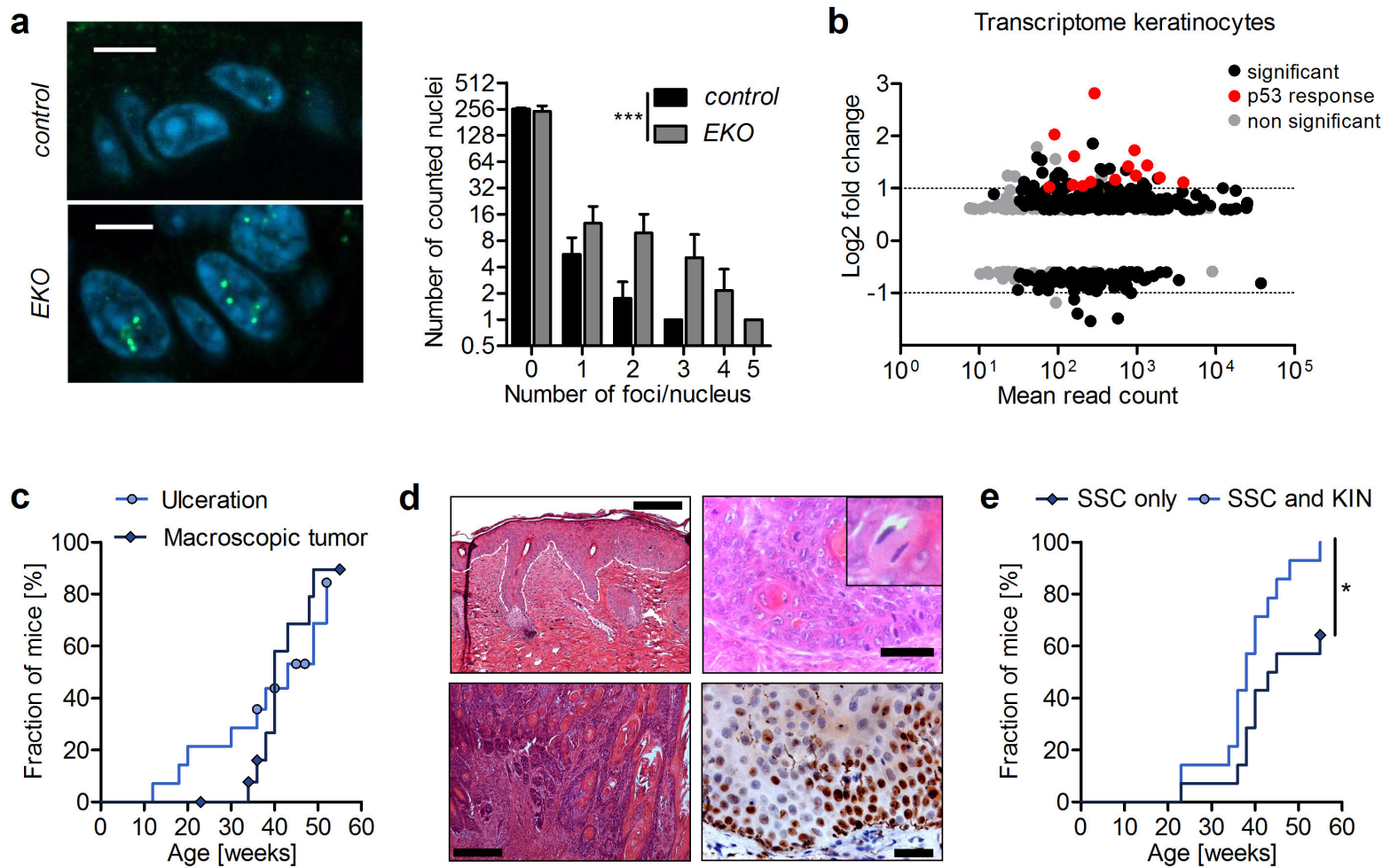


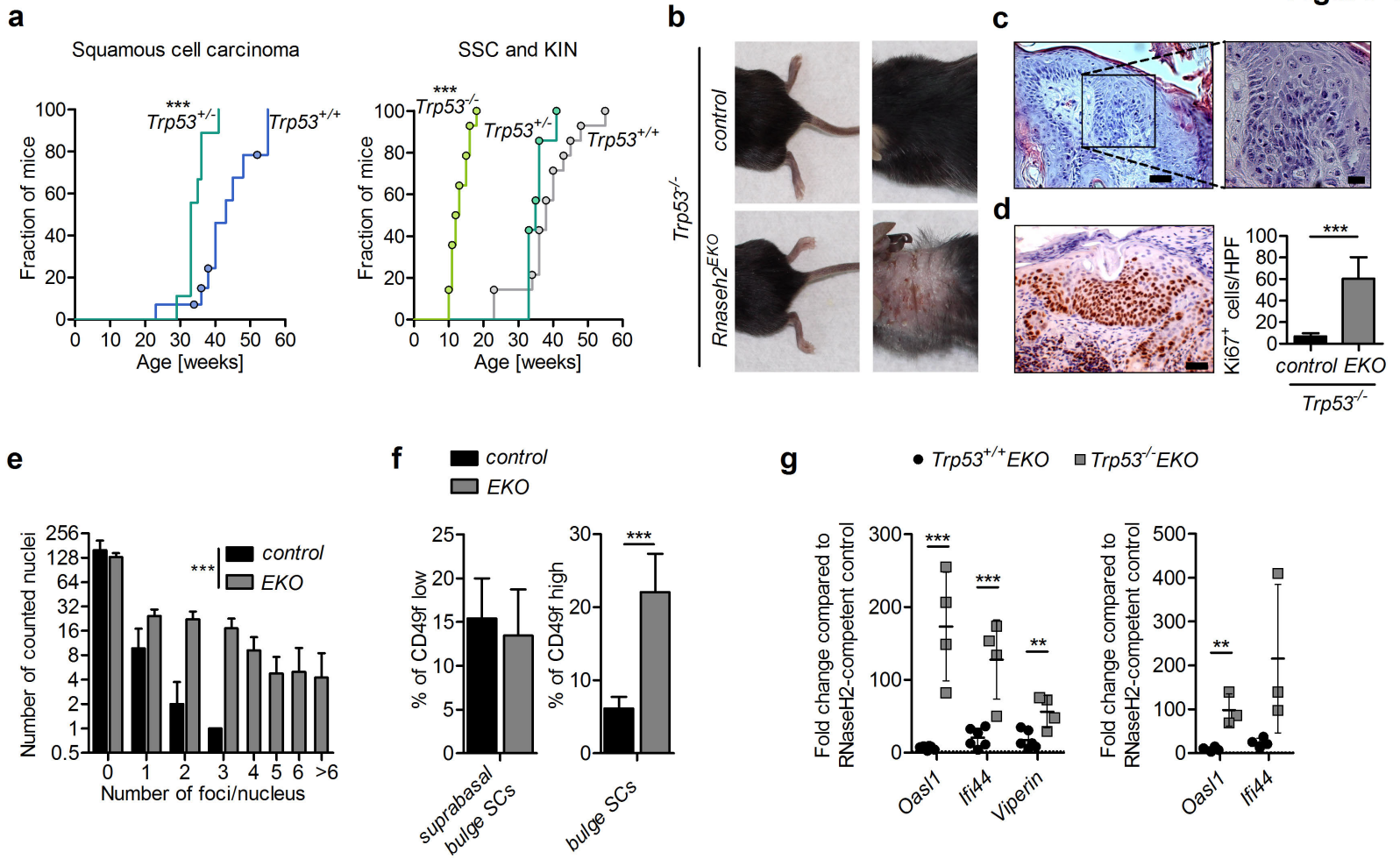
**Figure 2**





**Figure 3**



**Figure 4**

## Supplementary information.

### 1. Histopathological characterization of mutant skin

**Fig.1b. Back skin of 12 week-old *Rnaseh2<sup>EKO</sup>* mouse**, hematoxylin-eosin staining:

Acanthotic, hyperkeratotic epidermis with focal keratinocyte atypia.

**Fig.2a. Back skin of 7 week-old *Rnaseh2<sup>EKO</sup>* mouse**, anti-CD45 immunostaining:

Follicular hyperkeratosis associated with interface-dermatitis, i.e. hydropic degeneration of the lower epidermis and junctional infiltration of lymphoid immune cells. This inflammation pattern is typical of early SLE skin lesions.

**Fig.3d upper panels. *Rnaseh2<sup>EKO</sup>* back skin adjacent to spontaneous ulceration**, hematoxylin-eosin staining:

Advanced keratinocyte intraepithelial neoplasia (KIN III) in the peri-lesional skin: epidermal hyperplasia with full-thickness dysplasia, disordered dyspolarity, loss of maturation, and nuclear pleomorphism with hyperchromasia. Dyskeratotic cells and mitoses are present at all levels of the epidermis.

Classification of lesions into KIN I-III was according to Figueras et al.<sup>39</sup>. Briefly, KIN I is defined by Focal atypia of basal keratinocytes, involving only the lower third of the epidermis, KIN II by atypia of keratinocytes within the two lower thirds of the epidermis and KIN III by “full thickness dysplasia” with atypical cells extending to the upper layers.

**Fig.3d lower left. Macroscopic tumor in the genital area of a 36 week-old *Rnaseh2<sup>EKO</sup>* mouse**, hematoxylin-eosin staining:

Fully developed invasive squamous cells carcinoma. Invasion of the dermis by atypical keratinocytes with hyperchromatic nuclei. Tumor cells present with prominent mitotic activity, keratin pearl formation and premature cornification.

**Fig.4b. Hairless, inflamed and scaly back skin of a 15 week-old *Trp53<sup>-/-</sup>Rnaseh2<sup>EKO</sup>* mouse.**

KIN II. Irregular hyperplasia of the epithelium with keratinocyte atypia within the lower and middle layers of the epidermis. Prominent hyperchromatic nuclei and increased mitotic activity.

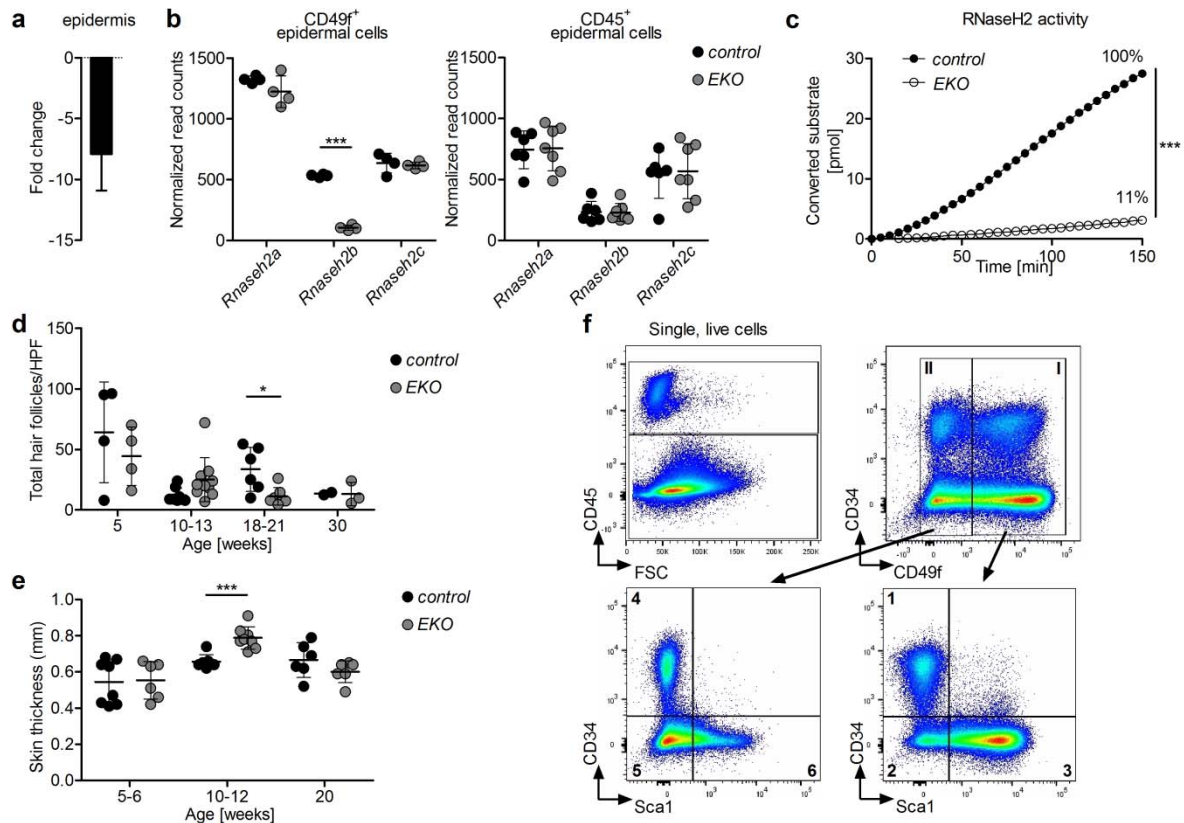


**Figure S1 (related to figure 1).** Efficient inactivation of RNase H2 in the epidermis, and skin phenotype of *Rnaseh2*<sup>EKO</sup> mice.

**a)** Quantification of *Rnaseh2b* mRNA levels in total epidermis of newborn *Rnaseh2*<sup>EKO</sup> mice (n=4) displayed as fold change compared to mean of control (*Rnaseh2b*<sup>FL/FL</sup>Cre-negative) littermates (n=4). The epidermal layer was separated from the underlying dermis by protease digest. Non-epithelial cells contained in the epidermis (melanocytes, immune cells) likely account for most of the residual *Rnaseh2b* mRNA in the *Rnaseh2*<sup>EKO</sup> mice.

**b)** Quantification of *Rnaseh2a*, *b* and *c* mRNA levels in populations FACS-purified from epidermal single cell suspensions of *Rnaseh2*<sup>EKO</sup> mice and control (*Rnaseh2b*<sup>FL/FL</sup>Cre-negative) littermates by mRNA sequencing. Left: CD45-negative  $\alpha 6$  integrin (CD49f)<sup>+</sup> epithelial cells; right: CD45<sup>+</sup> hematopoietic cells were sorted as a control population. Normalized numbers of reads mapping to the respective gene are shown. Each dot represents one mouse. Mean and SD, \*\*\* P<0.001.

**c)** RNase H2 activity in lysates of FACS-sorted keratinocytes (CD45-negative  $\alpha 6$  integrin<sup>+</sup>) from newborn *Rnaseh2*<sup>EKO</sup> mice (n=3) and control (*Rnaseh2b*<sup>FL/FL</sup>Cre-negative) littermates (n=4). Cleavage of a dsDNA substrate containing a single ribonucleotide was measured and activity was calculated from the slope of the graphs. Means are shown, \*\*\*<0.001 (two-way ANOVA).

**d)** Thickness of back skin folds of *Rnaseh2*<sup>EKO</sup> mice (*EKO*) and control (*Rnaseh2b*<sup>FL/FL</sup>Cre-negative) littermates (*ctrl*) determined using an engineer's caliper. Each dot represents one animal. Means and SD, \*\*\* P<0.001. Increased skin thickness at 10-12 weeks likely reflects abundance of hair follicles in anagen phase (associated with thicker dermal adipose tissue) in *Rnaseh2*<sup>EKO</sup> mice, whereas anagen follicles are virtually absent in control back skin at this time point.

**e)** Quantification of total numbers of hair follicles in back skin sections of *Rnaseh2*<sup>EKO</sup> mice and control (*Rnaseh2b*<sup>FL/FL</sup>Cre-negative) littermates. Means and SD.

**f)** Gating strategy for flow cytometric quantification of epidermal stem cell subpopulations in skin cell suspensions according to Jensen et al.<sup>54</sup>. **(1)** Bulge stem cells, **(2)** junctional zone stem cells, **(3)** infundibulum and interfollicular epidermis stem cells, **(4)** suprabasal bulge stem cells, **(5)** isthmus stem cells, **(6)** infundibulum and interfollicular epidermis stem cells.

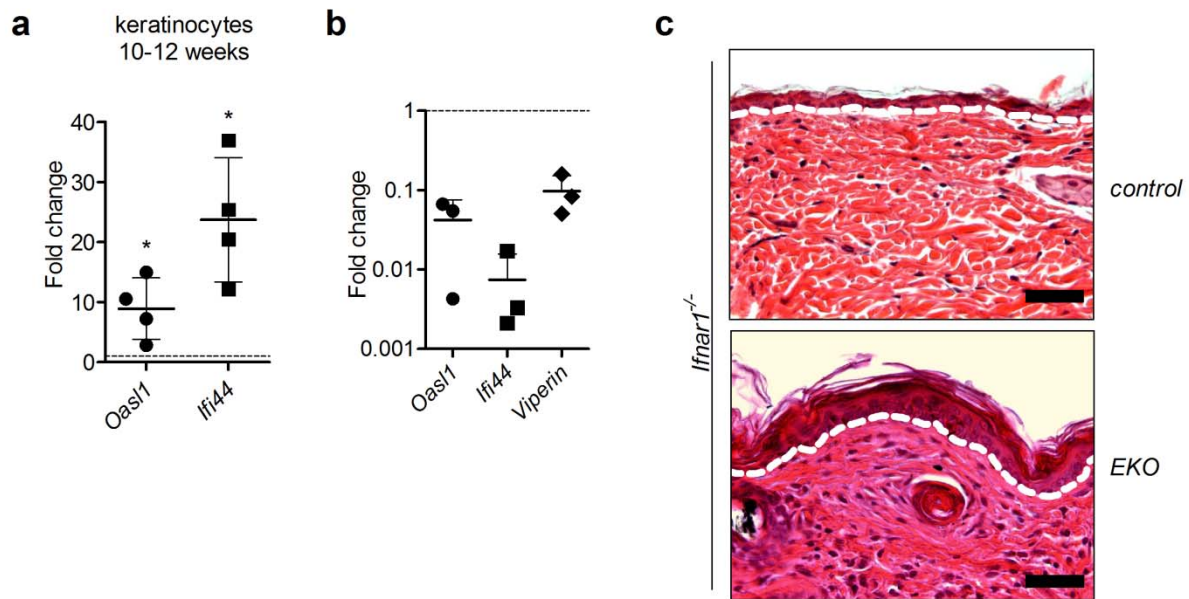


**Figure S2.** Spontaneous type I IFN response and inflammation in *Rnaseh2<sup>EKO</sup>* skin.

**a)** Comparison of ISG transcript levels determined by qRT-PCR in RNA extracted from keratinocytes FACS-purified from 10-12 week-old *Rnaseh2<sup>EKO</sup>* (*EKO*) mice (n=4) to the mean obtained for control (*Rnaseh2b<sup>FL/FL</sup>Cre*-negative) littermates (n=3) which was set to 1 (dotted line). \* P<0.05.

**b)** Control experiment demonstrating abrogation of type I IFN responses in *Rnaseh2<sup>EKO</sup>* mice deficient for the type I IFN receptor. *Rnaseh2<sup>EKO</sup>Ifnar1<sup>-/-</sup>* and IFNAR-competent *Rnaseh2<sup>EKO</sup>* mice were intraperitoneally injected with 200 µg polyI:C. 18 hours later, total RNA was extracted from spleen tissue and transcript levels of the indicated ISGs were determined by qRT-PCR. Means of IFNAR-competent controls were set to 1 (dotted line) and the fold difference of results obtained for *Rnaseh2<sup>EKO</sup>Ifnar1<sup>-/-</sup>* mice compared to this mean of controls is displayed.

**c)** Representative histology of back skin from a 11 week-old *Ifnar1<sup>-/-</sup>Rnaseh2<sup>EKO</sup>* mouse. Hematoxylin-eosin (H&E) staining shows that focal epithelial thickening and hyperkeratosis (thickening of cornified layer) characteristic of *Rnaseh2<sup>EKO</sup>* mice (Fig.1b) is not abrogated by additional inactivation of type I IFN-receptor expression. Scale bars 40 µm.



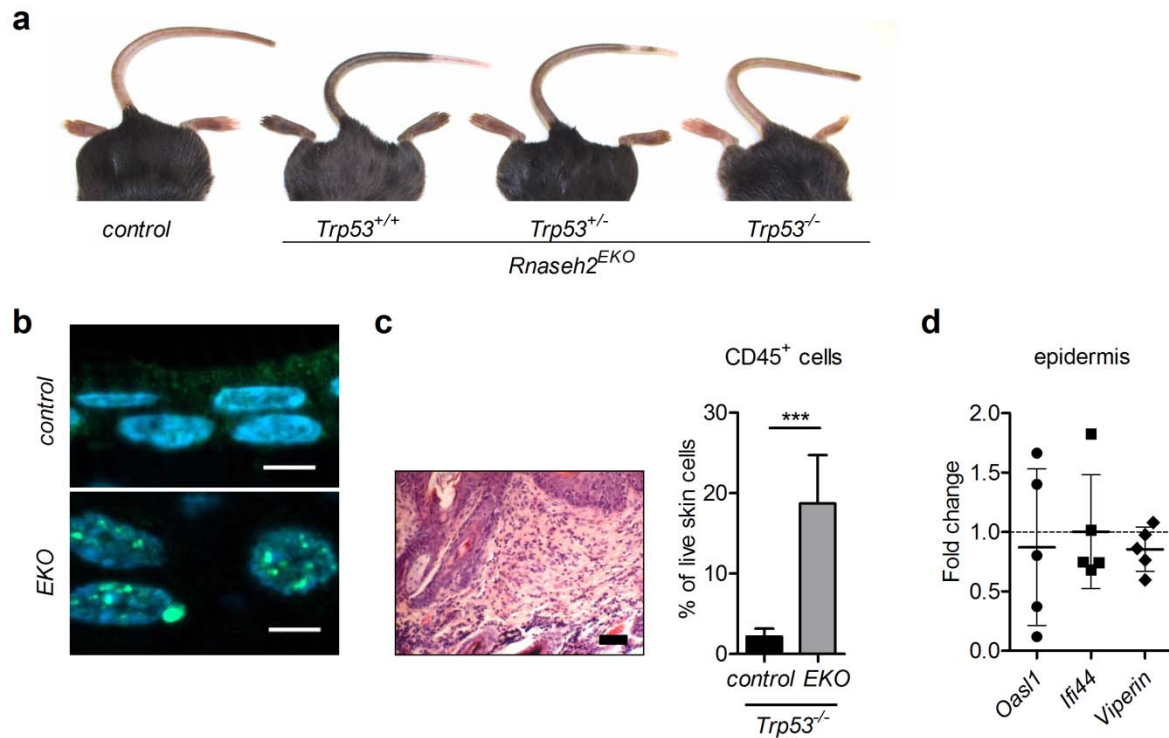


**Figure S4.** Influence of p53-deficiency on phenotype of  $Rnaseh2^{EKO}$  mice.

**a)** Comparison of macroscopic phenotypes of 12 week-old  $Rnaseh2^{EKO}$ ,  $Trp53^{+/-}Rnaseh2^{EKO}$ ,  $Trp53^{-/-}Rnaseh2^{EKO}$  animals. Note hyperpigmentation of tail, paws and ears depending on  $Trp53$  gene dose. Hair loss of the  $Trp53^{WT/WT}Rnaseh2^{EKO}$  animal is not yet manifest at this time point.

**b)** Representative images of  $Trp53^{-/-}Rnaseh2^{EKO}$  and control skin sections immunostained for  $\gamma$ H2AX. Note numerous repair foci indicating strand breaks in keratinocyte nuclei of the mutant skin. Scale bar 5  $\mu$ m.

**c)** Intense skin inflammation in an 11 week-old  $Trp53^{-/-}Rnaseh2^{EKO}$  mouse (Left). Note high number of nuclei in the dermal collagen representing mostly infiltrating immune cells. Scale bar 50  $\mu$ m. Quantification of CD45<sup>+</sup> leukocytes (right) in the epidermis of 10-12 week-old p53-deficient  $Rnaseh2^{EKO}$  ( $EKO$ ) mice (n=5) and control ( $Rnaseh2^{b^{FL/FL}Cre}$ -negative) littermates (n=5). Mean and SD, \*\*\*  $P < 0.001$ .

**d)** Control experiment excluding significant effects of p53-deficiency alone on type I IFN responses. ISG transcript levels were quantified by qRT-PCR in RNA extracted from total epidermis of 10-12 week-old animals. Graph shows results for  $Trp53^{-/-}$  animals in comparison to mean of wt controls (n=4), which was set to 1.

Gene_Symbol	log2FoldChange	padj
Ptgds	2,293	0
Ddit4l	2,409	0
Stfa1	2,289	0
Rhou	1,444	0,001
Ly6a	1,396	0,002
Klhl42	1,778	0,003
Irgm1	1,04	0,003
Ifi27l2a	1,694	0,003
Aoah	1,961	0,005
Ltf	1,933	0,005
Ly6f	1,457	0,006
Igfbp5	1,66	0,006
AW112010	1,081	0,006
Gbp5	1,778	0,01
Nppb	1,786	0,014
Tmem119	1,798	0,015
Serpinb3b	1,728	0,015
Mx1	1,773	0,016
Oasl1	1,686	0,019
Timp1	1,61	0,026
S100a9	1,697	0,026
Fbxo31	1,045	0,03
Ms4a6b	1,262	0,033
Pde7b	1,482	0,035
Rsad2	1,612	0,035
Ednrb	1,402	0,038
Ifitm1	1,407	0,041
Cxcl10	1,478	0,042
Lef1	1,552	0,044
Ifit3	1,503	0,044

**Table S1.** Transcripts have been identified as inducible by type I interferon using the Interferome v2.0 online tool.



Gene Symbol	log2FoldChange	padj
Abcb1b	2,813726278	1,35E-57
Ddit4l	2,025563734	1,17E-16
Ptp4a3	1,726522094	9,00E-21
Eda2r	1,6152473	5,00E-11
Ccng1	1,436712585	2,32E-17
Serpine2	1,417437977	5,77E-09
Ptgds	1,241128915	2,79E-21
Pmaip1	1,162864775	7,31E-13
Fos	1,111640973	3,31E-15
Mgmt	1,060691526	3,86E-06
Tnfrsf10b	1,041716403	2,17E-06
Fas	1,018445501	7,54E-05
Trp53inp1	1,205832504	8,23E-10

**Table S2.** Transcripts regulated by p53 in response to DNA damage have been identified using the Ingenuity Pathway Analysis (IPA) software (Qiagen).

***RNaseH2<sup>EKO</sup>* mice**

animal	age (wks)	macroscopic finding	histopathological diagnosis
60292	36	ulceration back	KIN3
60295	48	tumor ear	KIN2 with massive hyperkeratosis
60345	36	ulceration back	KIN2
60364	34	ulceration back	KIN2
60368	23	tumor neck	SSC grade 1-2
61572	40	ulceration back tumor mandibular/auricular region	KIN3 and SSC grade 1 SSC grade 1
61914	55	ulceration neck ulceration back ulceration ear	KIN3 KIN3 and SSC grade 1 KIN2
61915	38	ulceration neck/back hyperkeratotic tumor ear	KIN3 and SSC grade 1 KIN1
61918	45	tumor mandibular/auricular region	SSC grade 1-2
61919	38	tumor ear	SSC grade 1
62073	43	tumor ear	SSC grade 1
62166	36	tumor genital area	SSC grade 1-2
62168	23	ulceration neck/back	KIN2
62170	40	tumor mandibular/auricular region	SSC grade 2

**Table S3.** Histology of skin lesions (ulcerations or tumors) that required euthanasia of *RNaseH2<sup>EKO</sup>Trp53<sup>WT/WT</sup>* mice. Classification of lesions into KIN1-3 was according to Fernandez Figueras<sup>42</sup>.

***Rnaseh2b<sup>FL/FL</sup>K14-Cre<sup>+</sup>Trp53<sup>+/-</sup>***

animal	Age (wks)	macroscopic finding	histopathological diagnosis
64200	41	hyperkeratotic tumor ear	KIN III and initial SSC grade 1
64231	33	hyperkeratotic tumor ear	KIN III 3 and initial SSC grade 1
64527	36	hyperkeratotic tumor ear	SSC grade 1-2
64528	36	tumor ear tumor leg tumor abdomen	SSC grade 2 SSC grade 2 SSC grade 2
64646	33	hyperkeratotic tumor ear	KIN III and SSC grade 1
65162	33	tumor snout	SSC grade 1-2, (cystic growth pattern)
65163	29	tumor mandibular/auricular region	SSC grade 1-2, (cystic growth pattern)
65164	33	tumor ear	SSC grade 1
65165	35	tumor ear tumor leg	SSC grade 1-2 SSC grade 2

**Table S4.** Histology of skin tumors that required euthanasia of *RNaseH2<sup>EKO</sup>Trp53<sup>+/-</sup>* mice. Classification of lesions into KIN1-3 was according to Fernandez Figueras<sup>42</sup>.

***RNaseH2<sup>EKO</sup>Trp53<sup>-/-</sup>* and controls (*Rnaseh2b<sup>FL/FL</sup>* Cre-negative *Trp53<sup>-/-</sup>*)**

animal	genotype	age (wks)	histopathologic diagnosis
58544	control	11	no abnormality detected
64526	control	10	no abnormality detected
65705	control	11	no abnormality detected
65706	control	11	no abnormality detected
65711	control	11	no abnormality detected
66005	control	12	no abnormality detected
66006	control	12	no abnormality detected
66417	control	13	no abnormality detected
58644	<i>RNaseH2<sup>EKO</sup></i>	10	KIN II
59215	<i>RNaseH2<sup>EKO</sup></i>	10	KIN I
59222	<i>RNaseH2<sup>EKO</sup></i>	10	KIN I
64311	<i>RNaseH2<sup>EKO</sup></i>	11	KIN II
65707	<i>RNaseH2<sup>EKO</sup></i>	11	KIN I
66134	<i>RNaseH2<sup>EKO</sup></i>	11	KIN II
66654	<i>RNaseH2<sup>EKO</sup></i>	11	KIN II

**Table S5.** Histology of neck skin in *RNaseH2<sup>EKO</sup>Trp53<sup>-/-</sup>* and control (*Rnaseh2b<sup>FL/FL</sup>* Cre-negative *Trp53<sup>-/-</sup>*) mice aged 10-13 weeks. By this time, all *RNaseH2<sup>EKO</sup>Trp53<sup>-/-</sup>* mice had developed mildly hyperkeratotic and inflamed lesions in the neck that were itchy, while skin of littermate controls appeared normal. Classification of lesions into KIN1-3 was according to Fernandez Figueras<sup>42</sup>.

***RNaseH2<sup>EKO</sup>Trp53<sup>-/-</sup>***

animal	Age (wks)	histopathological diagnosis
59795	18	KIN III
60303	16	KIN II
61855	12	KIN II
61909	12	KIN II
63489	13	KIN III
63616	13	KIN III
64642	16	KIN III
64884	15	KIN III
64942	15	KIN III

**Table S6.** Neck skin of *RNaseH2<sup>EKO</sup>Trp53<sup>-/-</sup>* mice that had to be killed for exacerbation of the inflamed, hyperkeratotic skin lesions. Mice scratched extensively and neck skin was eroded. Classification of lesions into KIN1-3 was according to Fernandez Figueras<sup>42</sup>.